CrossMark

Studies on Spin Orbit Splitting and Dual Mode Phonon Vibrations in ZnS$_x$Se$_{1-x}$ Ternary Alloys Films with Varying Se Concentration

LALHRIATZUALA[1,2] and PRATIMA AGARWAL[1,3]

1.—Department of Physics, Indian Institute of Technology Guwahati, Guwahati 781 039, India.
2.—Department of Physics, Pachhunga University College, Aizawl 796 001, Mizoram, India.
3.—e-mail: pratima@iitg.ernet.in

ZnS$_x$Se$_{1-x}$ (x = 0, 0.41, 0.51, 0.91, 1) ternary alloy thin films with variable structural, optical and vibrational properties were prepared by thermal evaporation of solvothermally synthesized ZnS-ZnSe nanocomposite powders. The deposited films were uniform and have zinc-blende structure with (111) orientation. Variation of lattice parameter with composition was slightly nonlinear with a bowing parameter of 0.12 Å. Spin orbit (SO) splitting of the valence band was observed in binary ZnSe and ternary samples with large Se atomic concentration such as ZnS$_{0.41}$Se$_{0.59}$ and ZnS$_{0.51}$Se$_{0.49}$. The SO splitting energy decreases as the Se atomic concentration in the alloy decreases. Two phonon modes (corresponding to ZnS and ZnSe bonds) behavior were observed in the Raman spectra of the ternary alloys. The observed phonon mode frequencies shifted with changes in Se atomic concentration in agreement with theroretical predictions. Gap mode vibration of Se in ZnS lattice was also observed at 221 cm^{-1} in the ternary sample with small Se atomic concentration (ZnS$_{0.91}$Se$_{0.09}$), which also matches closely with theoretically calculated values.

Key words: II–VI ternary alloy, physical vapor deposition, dual mode phonon vibrations, spin orbit splitting

INTRODUCTION

ZnS$_x$Se$_{1-x}$ is one of the most technologically relevant II–VI alloy semiconductors. It is a very promising candidate for a wide variety of optoelectronic applications such as blue-green LEDs,[1,2] blue-green lasers,[3] photodetectors,[4] and as a buffer layer in thin film solar cells.[5] This is mainly due to its direct bandgap nature, tunable optoelectronic properties and flexibility in preparation techniques. The properties of the material can be tuned between the respective properties of the two end binary compounds, i.e., ZnSe and ZnS, simply by controlling the composition of the alloy.[6–8] This can be achieved by most thin film deposition processes such as pyrolitic spray deposition,[6] close-spaced sublimation,[7] plasma-induced isoelectric substitution,[8] metal organic vapour phase epitaxy (MOVPE),[9] atomic layer epitaxy (ALE),[10] etc.

The material, in addition to being very promising for many electronic applications, also possesses interesting optical and vibrational behaviors. Spin orbit (SO) coupling is a very important phenomenon, which affects the band structure in some of the II–VI compound semiconductors. This effect splits the valence band at the zone centre into Γ_7^v and Γ_8^v bands resulting in two direct optical transitions between the valence band and the conduction band, $(\Gamma_8^v \rightarrow \Gamma_6^c)$ and $(\Gamma_7^v \rightarrow \Gamma_6^c)$, respectively. The splitting effect has been reported for compounds with heavy anions such as CdTe,[11] ZnTe,[12] CdSe[13] and ZnSe.[11] The extent of the splitting in these materials is found to increase with the size of the

anion constituting the compounds. However, the effect is absent in those II–VI compounds, which are made up of smaller anions such as sulfide and oxide compounds. Since ZnS_xSe_{1-x} consists of sulfur and selenium, one of which is known to cause SO splitting, it is expected that the SO splitting phenomena may also occur in this alloy. Though the band structure of ZnS_xSe_{1-x} has not been well understood, the band gap of these alloys is experimentally observed to vary with alloy composition.[6–8] Study of the dependence of SO splitting on the fraction of sulfur content in the alloy will give a better understanding of the material property and may also help

in implementing the material for optoelectronic applications.

Two phonon modes is another interesting feature of ZnS_xSe_{1-x} compounds. As per theoretical predictions, the vibrational characteristic of both ZnS and ZnSe phonon modes are expected in the Raman spectra[14,15] of the ternary alloy. The frequency of these phonon modes is predicted to shift with compositional variation in such a way that the LO and TO modes of one of the constituting binary compounds merge together to form either gap mode or local mode, when the fraction of that anionic element responsible for the mode becomes very small.
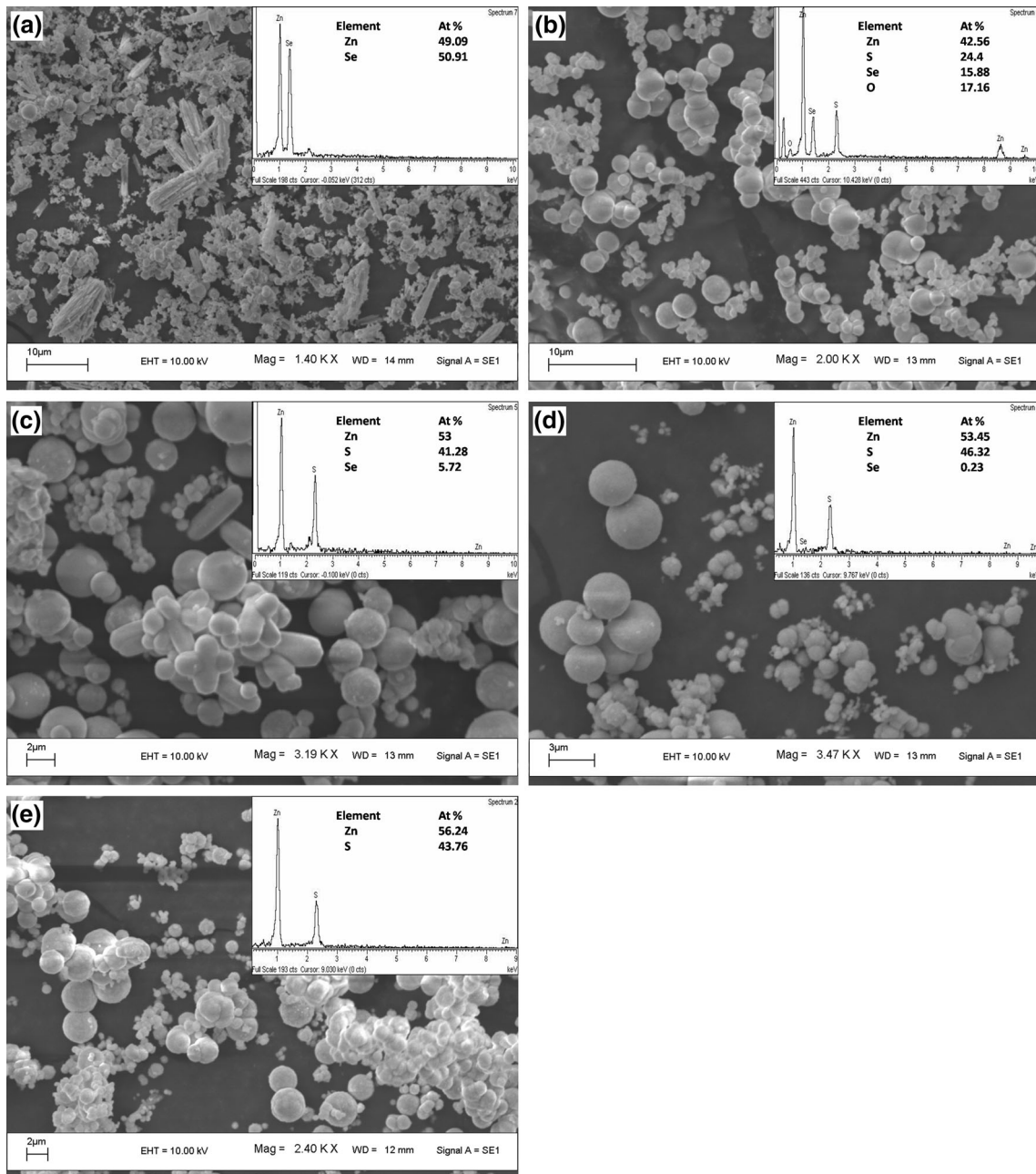

Fig. 1. SEM images and EDX spectra of the synthesized binary and composite nanoparticles, which are used as evaporation source for ZnS_xSe_{1-x} thin films: (a) $x = 0$, (b) $x = 0.41$, (c) $x = 0.51$, (d) $x = 0.91$, and (e) $x = 1$ respectively.

Studies on Spin Orbit Splitting and Dual Mode Phonon Vibrations in ZnS_xSe_{1-x} Ternary Alloys
Films with Varying Se Concentration

3343

A small fraction of sulfur in the ZnSe crystal is expected to form local mode vibrating almost independently at a frequency larger than the optical phonons of ZnSe. Similarly, a small fraction of Se in ZnS lattice is expected to result in gap mode vibrations.

In this work, we present our studies on ZnS_xSe_{1-x} thin films prepared by thermal evaporation of solvothermally synthesized ZnS-ZnSe composite powders. A systematic variation in structural and optical properties with composition has been experimentally observed for ternary alloy systems. SO splitting of the valence band is also observed in binary ZnSe and ternary samples with large Se atomic concentration such as $ZnS_{0.41}Se_{0.59}$ and $ZnS_{0.51}Se_{0.49}$. The SO splitting energy is found to decrease with the decrease in the Se atomic concentration in the alloy. Raman scattering studies have shown the presence of two-mode behavior in ternary alloys. The observed phonon mode frequencies are found to shift with changes in Se atomic concentration as theoretically predicted. In addition, gap mode vibration of Se in ZnS lattice was also observed at 221 cm^{-1} in the ternary alloy films with small Se atomic concentration, i.e., $ZnS_{0.91}Se_{0.09}$, which matches closely with theoretically calculated values.[14,16]

EXPERIMENTAL

ZnS_xSe_{1-x} thin films ($x = 0, 0.41, 0.51, 0.91, 1$) were prepared on Corning 1737 glass by thermal evaporation of solvothermally synthesized ZnS-ZnSe composite powders. In the solvothermal synthesis, zinc acetate [$(CH_3COO)_2Zn \cdot 2H_2O$], sodium sulfite [$Na_2SO_3$] and sodium selenite [$Na_2SeO_3$] were used as a precursor for zinc, sulfur and selenium ions, respectively. A mixed solution made up of appropriate amounts of ammonia ($NH_3 \cdot H_2O$), hydrazine hydrates ($N_2H_4 \cdot H_2O$) and de-ionzed water was used as a solvent. The synthesis process follows the usual solvothermal route similar to the process described in the literature.[17,18] All the powders were prepared at 180°C furnace temperature for 5 h reaction time. For each of the binary (ZnS and ZnSe) and ternary alloy films (with $x = 0.41$, 0.51 and 0.91), the respective evaporation sources, i.e., ZnS and ZnSe powders and ZnS-ZnSe composite powders, were synthesized using different molar ratios of the anion salts to vary the relative concentrations of Se and S atoms in the alloy. To obtain the alloy thin films with different compositions, the powders were then thermally evaporated using a molybdenum boat in a vacuum chamber. All the films were deposited at a fixed substrate temperature of 200°C on Corning 1737 glass substrates.

Compositions of synthesized powders and thin films were obtained by energy dispersive x-ray spectroscopy (EDAX) attached to a scanning electron microscope (SEM; LEO 1430 VP). Surface morphology of the films was studied using a Field Emission Scanning Electron Microscope (FESEM; ΣIGMA ZEISS). A HORIBA JOBIN–YVON Lab-RAM HR spectrometer was used to record room-temperature Raman spectra. An Ar ion laser with excitation wavelength of 488 nm and 18 mW power was used for all the measurements. The spectral transmittance of the films was recorded between 220 and 2500 nm using aUV–Vis-NIR spectrophotometer (Shimadzu UV 3101PC). The thickness measurements were performed using a Stylus profilometer. X-ray diffraction (XRD) patterns were recorded in 2θ range of 20°–65° using Cu-Kα radiation ($\lambda = 1.54$ Å). Crystallite size, lattice strain and dislocation density of the films were obtained from the XRD patterns using the following relationships[19]:
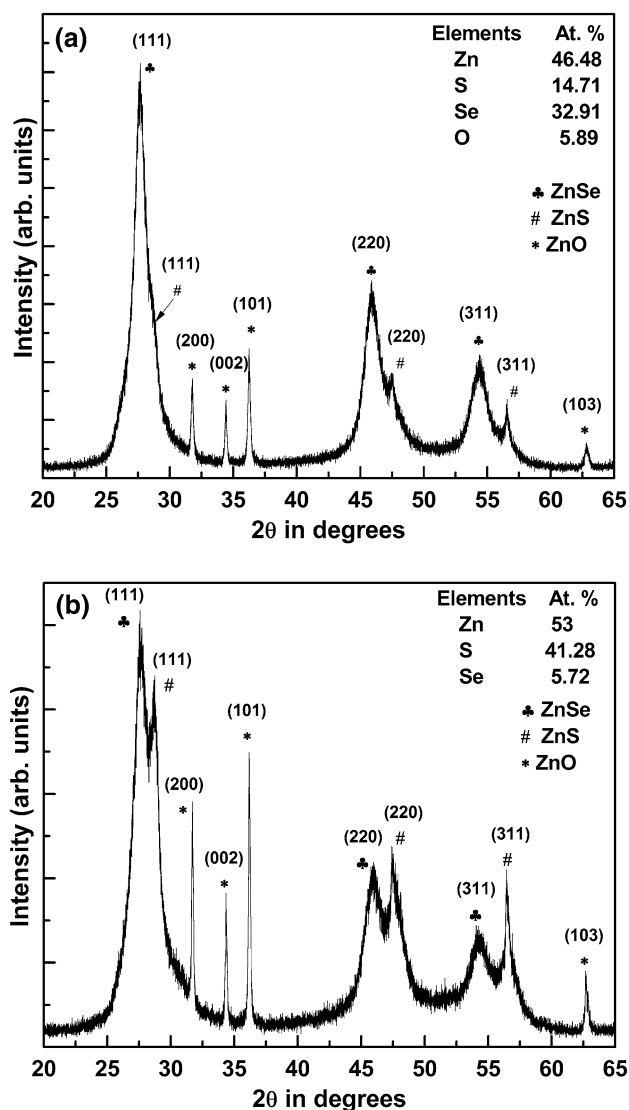

Fig. 2. XRD patterns of the synthesized composite nanoparticles showing diffraction peaks from ZnS and ZnSe: evaporation source of (a) $x = 0.41$ and (b) $x = 0.51$ thin films respectively.
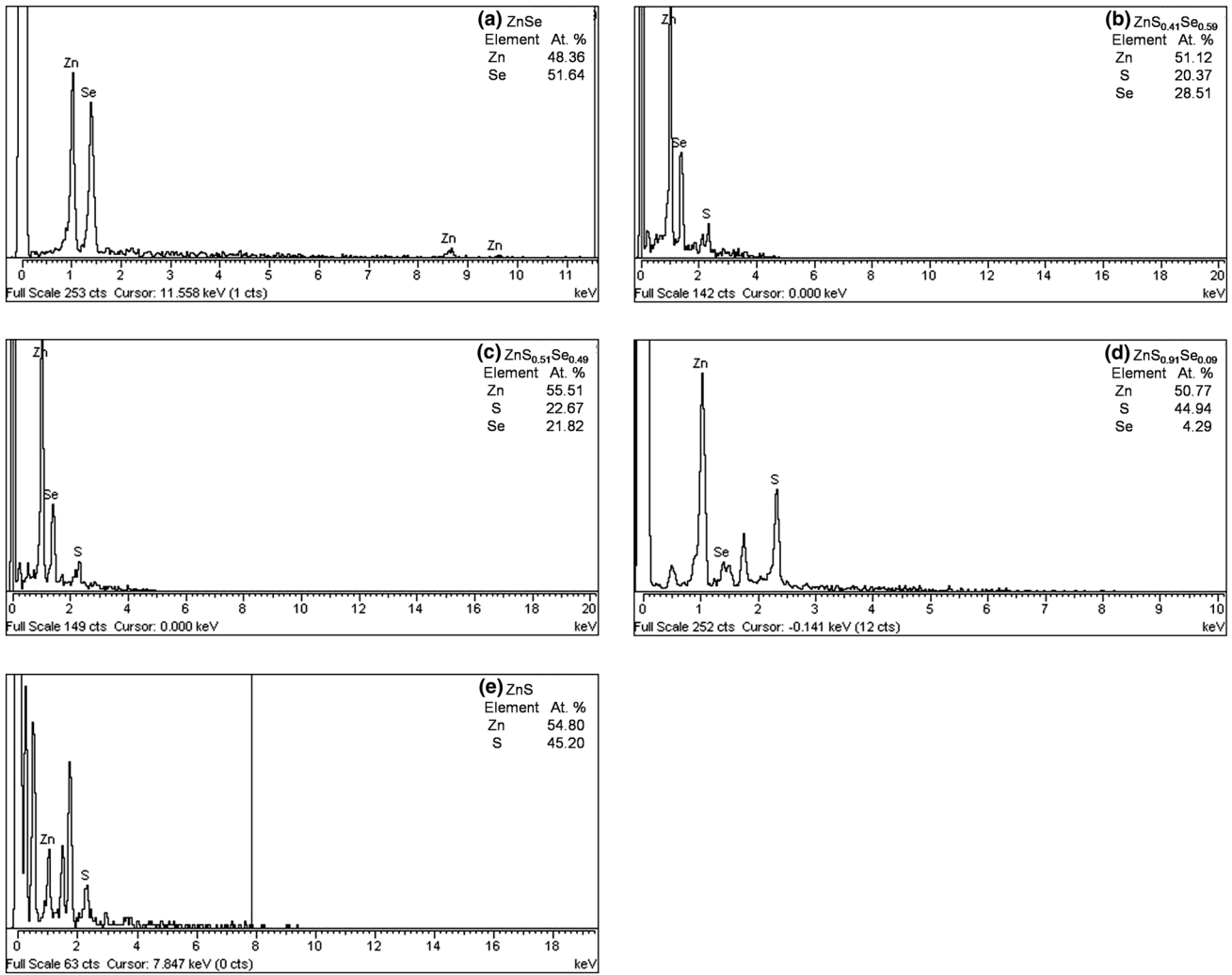
Fig. 3. EDX spectra of the prepared ZnS_xSe_{1-x} thin films: (a) $x = 0$, (b) $x = 0.41$, (c) $x = 0.51$, (d) $x = 0.91$, and (e) $x = 1$ respectively.

Crystallite size, $\quad D = \dfrac{K\lambda}{\beta \cos\theta}$ (1)

(Debye Sherrer's formula)

where $K(\sim 0.9)$ is a dimensionless shape factor and β is the full width at half-maxima (FWHM).

Lattice strain, $\quad \varepsilon = \dfrac{\beta \cos\theta}{4}$ (2)

Dislocation densities, $\quad \delta = \dfrac{1}{D^2}$ (3)

RESULTS AND DISCUSSION

Figure 1a–e shows the SEM images and the corresponding EDX spectra of the synthesized ZnS-ZnSe nanocomposite powders. The compositions are an average of the measurements taken over 2–3 different positions in the SEM images. In addition to zinc, sulfur and selenium, traces of oxygen are also present in the synthesized powders. XRD patterns of the synthesized composite powders (Fig. 2a and b) show diffraction peaks corresponding to the cubic planes of both ZnSe and ZnS, which indicates the composite nature of the synthesized powders.
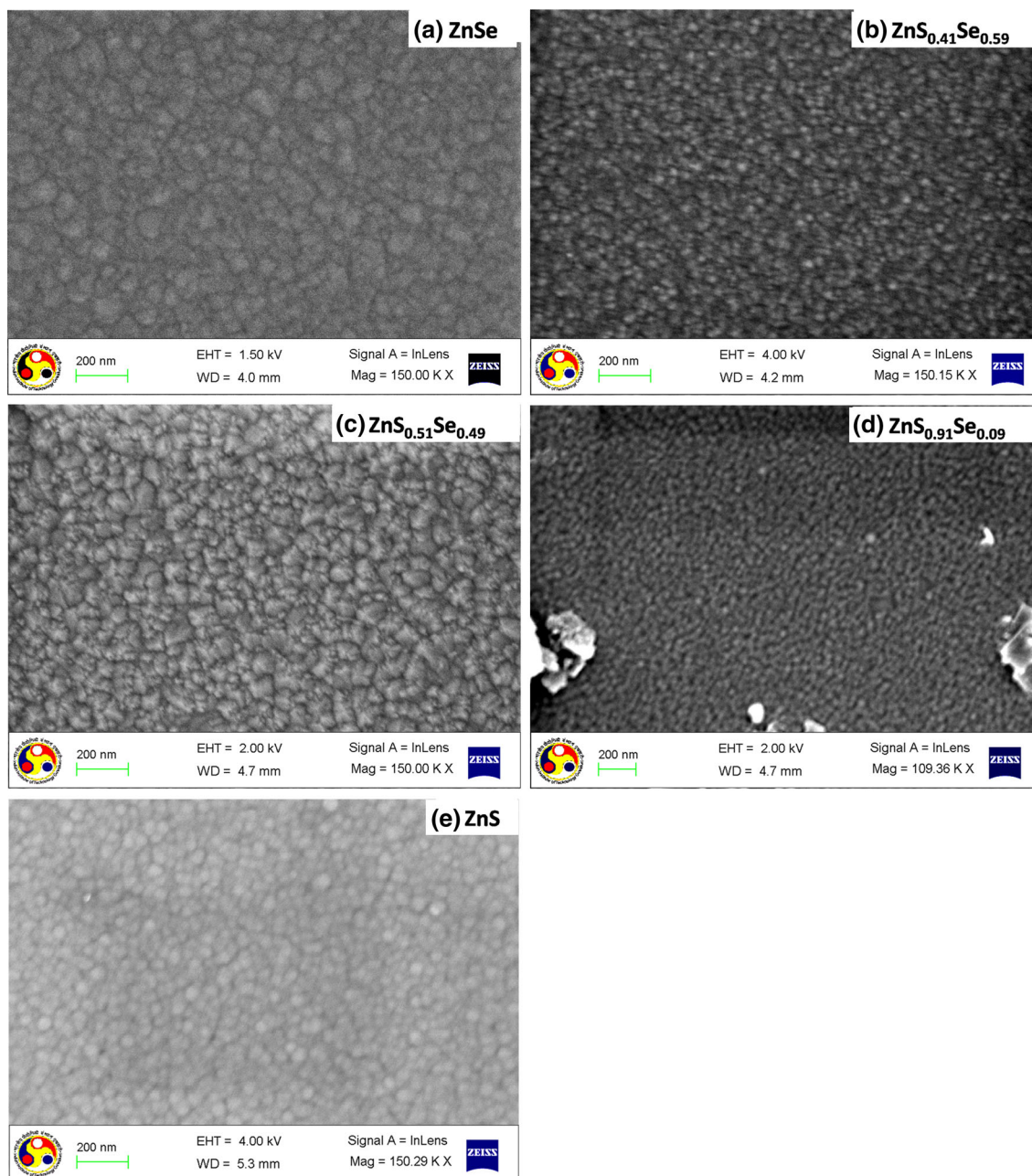
Studies on Spin Orbit Splitting and Dual Mode Phonon Vibrations in ZnS_xSe_{1-x} Ternary Alloys Films with Varying Se Concentration

3345

Fig. 4. FESEM images of ZnS_xSe_{1-x} ($x = 0, 0.41, 0.51, 0.91, 1$) alloy thin films: (a) $x = 0$, (b) $x = 0.41$, (c) $x = 0.51$, (d) $x = 0.91$, and (e) $x = 1$ respectively.

Figure 3a–e shows the EDX spectra of the films. The atomic percentage of different ions shown in this case are also averaged over 2–3 measurements at different locations on the films. Except for ZnSe, all the remaining films appear to be slightly Zn rich. The fraction of sulfur content (x) in the films is obtained by normalizing the total atomic percentage of anion content in the films. It is observed here that the films do not maintain the same composition as the source material. This may be understood by looking at the phenomena involved in our sample

preparation process. Although the mechanism involved in the thermal evaporation process is quite simple and well understood, our preparation process, however, involves evaporation of composite powders consisting of two different binary alloy compounds with different vapour pressures. The crystal growth in the thermal evaporation process is largely determined by the rate of solid transport. The number of molecules (n) striking a surface of the substrate per unit area per unit time is related to the vapour pressure (p) as $n = (2\pi mkT)^{-1/2} \cdot p$,

where m is the molecular mass, and T is the absolute temperature.[20] Since the vapour pressure of ZnSe is higher than the vapour pressure of ZnS,[21] it therefore results in unequal amounts of ZnS and

ZnSe molecules striking the surface of the substrate even for the same amount of the two materials. Hence, the formation of Zn–Se bonding in the resulting alloy is more favourable than Zn-S, and, thus, the compositions of the resulting alloys do not match with the source composite powders.

FESEM images of the films are shown in Fig. 4. The films are deposited uniformly throughout the surface and consist of densely packed small grains without any pinholes. $ZnS_{0.41}Se_{0.59}$, $ZnS_{0.91}Se_{0.09}$ and ZnS samples consist of small and spherical-shaped grains with an average diameter of around 50 nm. ZnSe and $ZnS_{0.51}Se_{0.49}$ samples, on the other hand, have much bigger irregular-shaped grains of almost 100 nm diameter. Thus, the dimension of the grains and, hence, the quality of the film surface is not monotonically varying with composition. Though the reason for this is not very clear, it could be due to some variation in substrate temperature during deposition.

Figure 5a shows the XRD patterns of ZnS_xSe_{1-x} thin films ($x = 0$, 0.41, 0.51, 0.91, and 1). Contrary to the powder samples, where we observed peaks corresponding to the crystal planes of both ZnS and ZnSe, only one distinct characteristic peak corresponding to the (111) plane of zinc blende structure (PDF #800021, PDF #772100) of the compound is observed. With the changing composition, the 2θ value of the diffraction peak shifts from 27.26° in ZnSe ($x = 0$) film to 28.62° in ZnS ($x = 1$) film.

Structural parameters of the alloys calculated from the (111) plane using the Debye–Sherrer formula are given in Table I. The lattice constant 'a' of the films decreases from 5.662 Å to 5.398 Å as x increases from 0 to 1. As shown in Fig. 5b, this variation of lattice constant with composition nearly follows a linear Vegard's relationship, but with small deviations. Although most mixed crystals have been assumed to follow the empirical Vegard's relationship, deviation from the linear relationship has been observed both experimentally and theoretically.[22–24] This could be due to large lattice parameter differences of the constituting binary compounds and non-linear variation of cell volume with compositional changes. The observed lattice parameter variation given in Fig. 5b follows a second-order polynomial relationship, $a_{ZnS_xSe_{1-x}} = (1-x)a_{ZnSe} + xa_{ZnS} - x(1-x)b$, with a bowing parameter b equal to 0.12 Å.
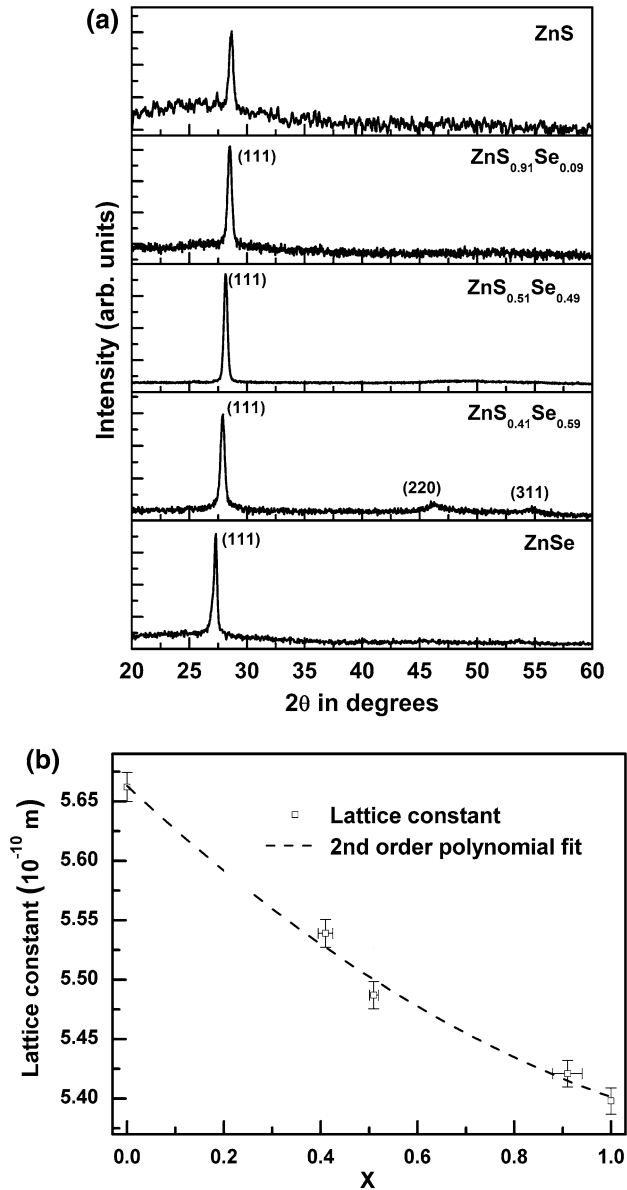
Fig. 5. (a) XRD pattens of ZnS_xSe_{1-x} thin films ($x = 0$, 0.41, 0.51, 0.91, 1). (b) Plot of lattice constant (a) versus sulfur content (x).

Table I. Structural parameters of ZnS_xSe_{1-x} thin films

Sample	2θ (°)	β (FWHM) (°)	Lattice constant 'a' (Å)	Lattice strain	Dislocation density (lines/m^2)	Average crystallite size (nm)
ZnSe	27.260	0.316	5.662	1.34×10^{-3}	1.37×10^{15}	27
$ZnS_{0.41}Se_{0.59}$	27.880	0.395	5.539	1.67×10^{-3}	2.13×10^{15}	22
$ZnS_{0.51}Se_{0.49}$	28.150	0.309	5.487	1.30×10^{-3}	1.30×10^{15}	28
$ZnS_{0.91}Se_{0.09}$	28.500	0.386	5.421	1.63×10^{-3}	2.03×10^{15}	22
ZnS	28.625	0.376	5.398	1.59×10^{-3}	1.93×10^{15}	23

Studies on Spin Orbit Splitting and Dual Mode Phonon Vibrations in ZnS$_x$Se$_{1-x}$ Ternary Alloys Films with Varying Se Concentration
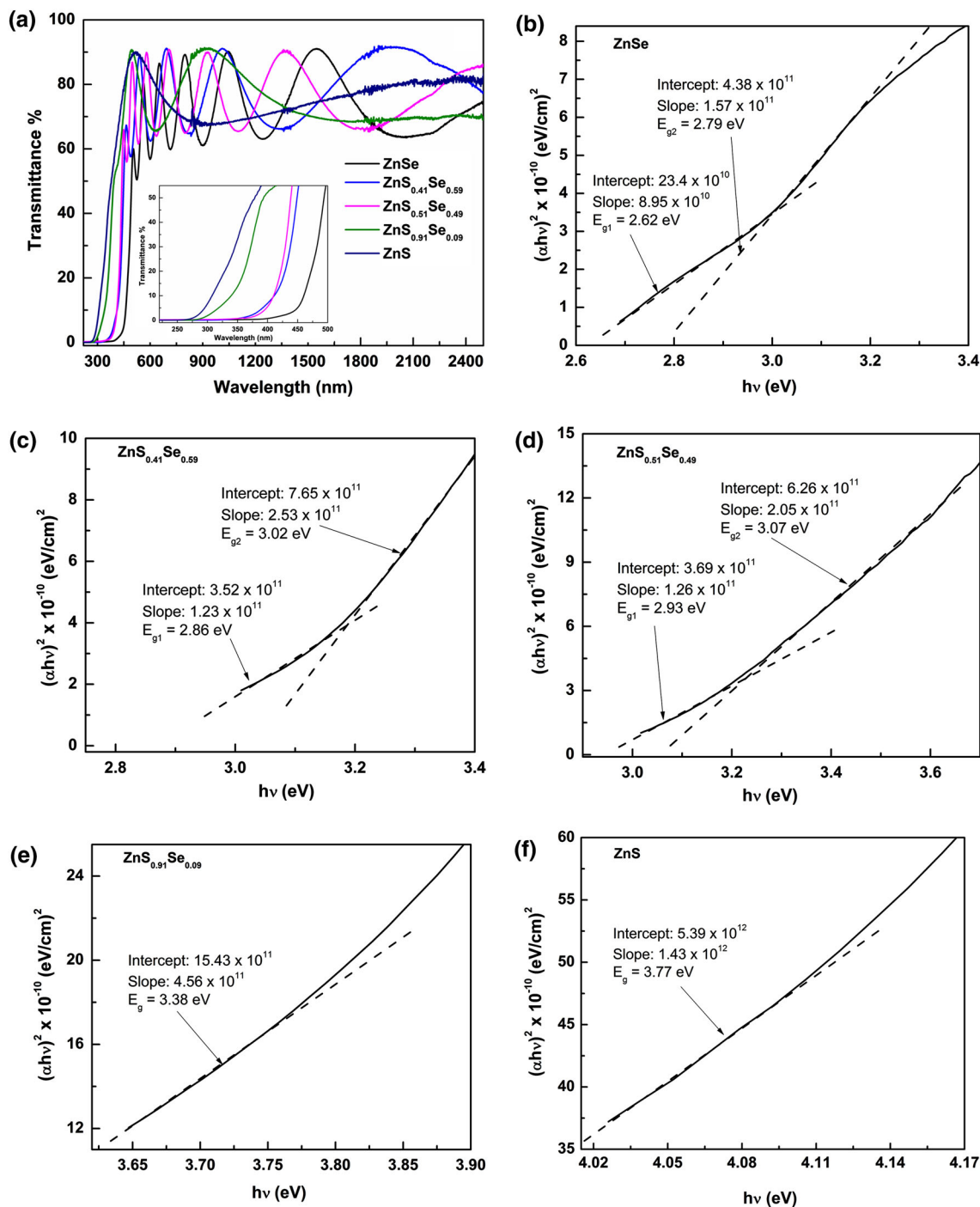
3347

Fig. 6. (a) UV–Vis-NIR transmission spectra of ZnS$_x$Se$_{1-x}$ thin films (x = 0, 0.41, 0.51, 0.91, 1), (b–f) ($\alpha h\nu$)^2 versus $h\nu$ plot.

The calculated lattice strain and dislocation density of the films are given in Table I. These parameters correlate with the grain size of the particles. Samples with larger grains such as ZnSe and ZnS$_{0.51}$Se$_{0.49}$ have lower lattice strain and dislocation densities in comparision to the other three samples. The average crystallite size varies from 20 nm to 27 nm, which is much smaller than the grain sizes observed in the FESEM images. Since it

is not possible to isolate the size and strain broadening from a single diffraction peak,[25] the average crystallite size as obtained from the Debye–Sherrer formula is likely to be underestimated, whereas the strain and dislocation density may be slightly overestimated.

Figure 6a shows the UV–Vis-NIR transmission spectra of the thin films at normal incidence. All the films show good interference patterns in the NIR
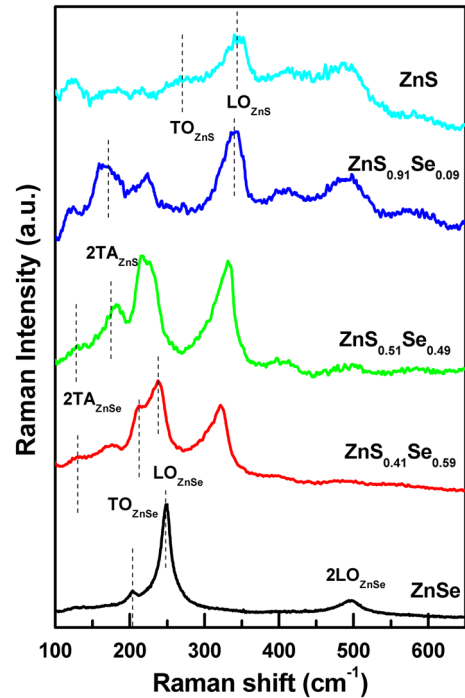
Table II. Band gap, refractive index and film thickness of ZnS_xSe_{1-x} alloy thin films

Sample	Film thickness (nm)		n (550 nm)	E_{g1} ($\Gamma_8^v \to \Gamma_6^c$) (eV)	E_{g2} ($\Gamma_7^v \to \Gamma_6^c$) (eV)	S–O splitting (eV)
	UV data	Profilometer				
ZnSe	640	670	2.61	2.62	2.79	0.17
$ZnS_{0.41}Se_{0.59}$	432	500	2.48	2.86	3.02	0.16
$ZnS_{0.51}Se_{0.49}$	590	550	2.45	2.93	3.07	0.14
$ZnS_{0.91}Se_{0.09}$	200	200	2.43	3.38		0
ZnS		152		3.77		0
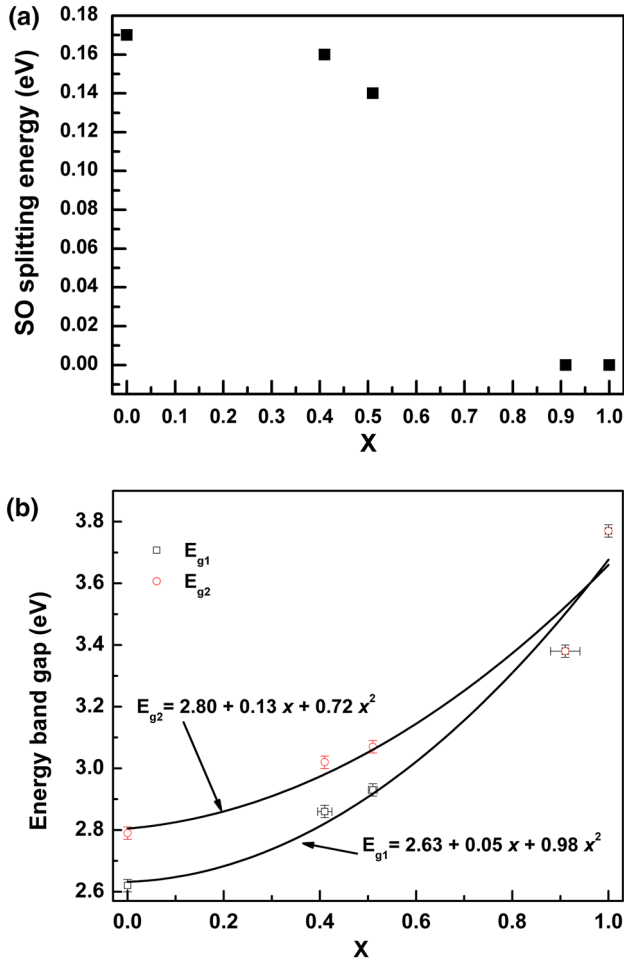
Fig. 7. (a) Plot of SO splitting energy versus fraction of sulfur (x), (b) plot of energy bandgap versus fraction of sulfur (x).

Fig. 8. Raman spectra of ZnS_xSe_{1-x} ($x = 0, 0.41, 0.51, 0.91, 1$) thin films.

region with a maximum transmittance of about 90% indicating that the films are uniformly deposited on the substrate. The optical absorption edge, as indicated by a sharp drop in the transmittance spectra, moves towards shorter wavelengths with increasing x.

Optical parameters such as the refractive index (n), absorption coefficient (α) and thickness of the films are determined from the transmission spectra using the method described by Swanepoel.[26] From these parameters, we obtain $(\alpha h v)^2$ versus $h v$ plot as given in Fig. 6b–f. The linear dependence of $(\alpha h v)^2$ on $h v$ in the plot indicates the occurrence of direct optical transition as expected in these semiconductors. The bandgaps corresponding to each direct optical transitions are obtained by fitting a straight line as shown in the figures. The values obtained from these fittings are given in Table II. The binary sample ZnSe and the ternary samples with a significant fraction of selenium atoms, $ZnS_{0.41}Se_{0.59}$, and $ZnS_{0.51}Se_{0.49}$, posses two bandgaps, E_{g1} and E_{g2}, corresponding to two direct optical transitions, ($\Gamma_8^v \to \Gamma_6^c$) and ($\Gamma_7^v \to \Gamma_6^c$). However, the remaining two samples with very small amounts of Se, $ZnS_{0.91}Se_{0.09}$ and ZnS possess only one bandgap. The bandgap values for the binary compounds, ZnSe and ZnS, are comparable to the respective values as reported in the literature.[19,27,28]
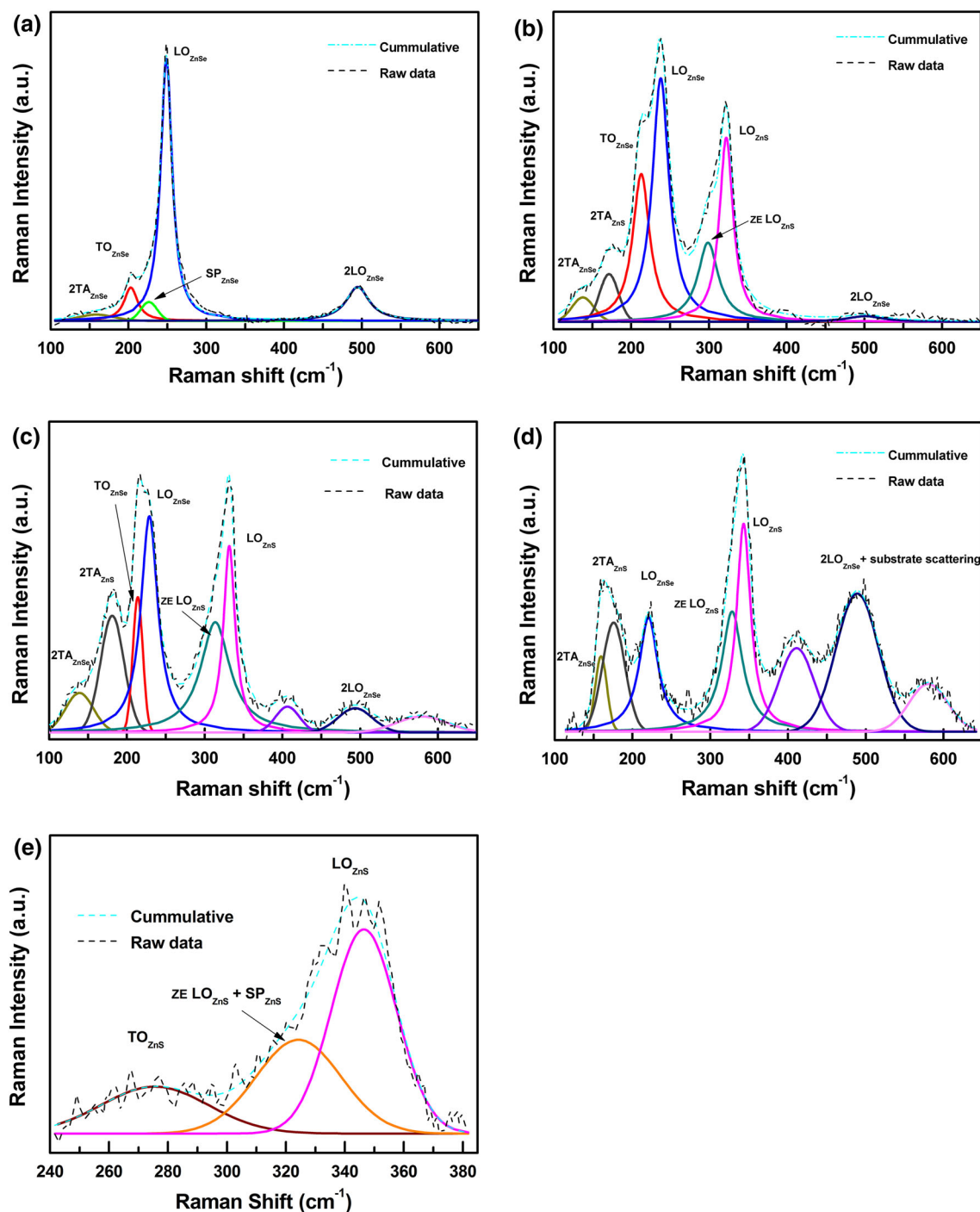
Fig. 9. Deconvoluted Raman spectra of ZnS$_x$Se$_{1-x}$ (x = 0, 0.41, 0.51, 0.91, 1) thin films: (a) x = 0, (b) x = 0.41, (c) x = 0.51, (d) x = 0.91, and (e) x = 1 respectively.

The observed two direct optical transitions in ZnSe have been reported both theoretically and experimentally.[11,29] However, for ternary compounds, the occurrence of two direct optical transitions has not been reported to the best of our knowledge. The reported ZnSe band structure calculations[11] have shown that the valence band splits at the zone centre into Γ_7^v and Γ_8^v resulting in two direct optical transitions as reported in this work.

This splitting is, however, absent in the band structure of ZnS.[30] This splitting is due to the SO coupling effect in the valence band, often observed in compounds consisting of anions with large ionic radii such as CdSe, CdTe, etc.[11,13,31] In these materials, the nearly relativistic electronic velocities lead to sufficiently large magnetic fields so that the magnetic moments of orbital motion and the spin motion interact, which result in spin–orbit coupling.

Table III. Phonon modes of ZnS_xSe_{1-x} ($x = 0, 0.41, 0.51, 0.91, 1$) thin films

Phonon mode	ZnSe			$ZnS_{0.41}Se_{0.59}$			$ZnS_{0.51}Se_{0.49}$			$ZnS_{0.91}Se_{0.09}$			ZnS		
	Band centre (cm^{-1})	FWHM (cm^{-1})	Intensity	Band centre (cm^{-1})	FWHM (cm^{-1})	Intensity	Band centre (cm^{-1})	FWHM (cm^{-1})	Intensity	Band centre (cm^{-1})	FWHM (cm^{-1})	Intensity	Band centre (cm^{-1})	FWHM (cm^{-1})	Intensity
$2TA_{ZnSe}$	159	53.7	151	138	33.1	149	139	42.2	116	159	17.8	245			
$2TA_{ZnS}$				171	28.5	292	181	35.7	341	176	34.5	354			
TO_{ZnSe}	203	21.1	805	213	26.5	903	214	15.2	396						
SP_{ZnSe}	226	25.0	454												
LO_{ZnSe}	249	17.9	6317	238	26.1	1489	229	26.4	633	221	29.3	371			
TO_{ZnS}													275	43.0	39
$ZE\ LO_{ZnS}$				299	31.9	484	313	46.1	321	328	32.4	389	324	34.0	78
LO_{ZnS}				322	21.2	1125	332	18.2	547	343	21.9	674	346	26.1	170

However, in the materials consisting of only light anions such as ZnS, CdS, etc., the magnetic field generated by orbiting electron is too weak to induce any coupling with electron spin.

SO splitting energy of all the samples is calculated from the difference in the energies of the two bandgaps, E_{g1} and E_{g2}. It is plotted against the fraction of sulfur (x) in Fig. 7a. The plot shows that, in addition to the well-known SO splitting in ZnSe, significant SO splitting is observed even in ternary samples with a large fraction of Se.

Figure 7b shows the bandgap energy versus x plot. Dependence of the bandgap on the composition of the alloy is non-linear as predicted by Vegard's law. The second-order polynomial fitting of E_{g1} and E_{g2}, both shown in the figure, results in bowing parameters of 0.98 and 0.72 eV, respectively. This bowing is mainly due to the difference in bond lengths of the ZnS and ZnSe bonds. In ternary alloys, this difference alters the bond angles in order to preserve the bond lengths. This perturbs the atomic potentials, which results in non-linear variation of bandgap energy even with uniform substitution of the constituent elements.

The vibrational properties of the films are studied using Raman scattering measurements. Since all the films have zinc blende structure with (111) orientation, scattering from both transverse optical (TO) and longitudinal optical (LO) phonons are permitted in these measurements. The room-temperature Raman spectra are shown in Fig. 8. The ZnSe thin film has distinct vibrational bands corresponding to TO_{ZnSe}, LO_{ZnSe} and $2LO_{ZnSe}$ phonons. The spectra of all the ternary samples exhibit prominent Raman bands corresponding to both ZnSe and ZnS like phonons as predicted by a modified random element isodisplacement model (MREI).[14] However, with the increase in the fraction of sulfur in the film, not only the intensity of ZnS-like phonon mode increases but we also observe an increase in the intensity of disorder-induced phonons (2TA and zone edge LO phonon modes for ZnS) and the scattering from the substrate. This substrate scattering largely dominates the Raman spectra of the ZnS thin films, which are relatively thin, as shown in the figure. Nevertheless, weak TO_{ZnS} and asymmetric LO_{ZnS} can still be identified from the spectra as indicated.

For detailed investigation of different vibrational modes, all the Raman spectra are deconvoluted into the individual phonon modes of ZnS and ZnSe. Figure 9a–e shows the deconvoluted spectra. Except for the ZnS sample, the zone centre ($k = 0$) phonons are fitted with a Lorentzian peak and the disorder-activated phonons with a Gaussian peak. Since the ZnS film is highly nanocrystalline, all the three phonon modes in ZnS are best fitted with the Gaussian peak. In all the fittings, the cumulative fits and the raw data match very well as shown in the figures. Table III shows the band centre position, the full-width at half-maxima (FWHM) and the intensity of

Studies on Spin Orbit Splitting and Dual Mode Phonon Vibrations in ZnS_xSe_{1-x} Ternary Alloys
Films with Varying Se Concentration

3351

the observed phonon modes. All the phonon modes including the zone centre phonons have FWHM, which is comparatively much larger than the bulk values of about 7–8 cm^{-1} as reported for the II–VI binary compounds.[32] The LO and TO phonon modes of both ZnSe and ZnS are slightly red-shifted from the reported values (reported values are at TO_{ZnSe} = 205 cm^{-1},[33–35] LO_{ZnSe} = 250 cm^{-1},[33] TO_{ZnS} = 277 cm^{-1},[36] LO_{ZnS} =350 cm^{-1} [36,37]).

Strong first-order zone centre phonons such as TO_{ZnSe}, LO_{ZnSe} and LO_{ZnS} are observed in the deconvoluted spectra of two of the ternary alloys with large fractions of Se ($ZnS_{0.41}Se_{0.59}$ and $ZnS_{0.51}Se_{0.49}$). But the third ternary sample, i.e., $ZnS_{0.91}Se_{0.09}$ exhibits phonon mode, LO_{ZnS}, and only one ZnSe-like phonon mode at 221 cm^{-1}. The LO_{ZnS} in all these ternary alloy samples have asymmetric broadening towards the lower wave number side. It is fitted with an additional Lorentzian peak, which is identified as a zone edge LO phonon (ZE LO_{ZnS}). Similar asymmetric broadening is also observed in the zone centre LO_{ZnSe} and LO_{ZnS} phonons in the binary compounds (ZnSe and ZnS). The asymmetric broadening in both of these binary samples fits well with an additional Gaussian peak as shown in the deconvoluted spectra. These are identified as SP_{ZnSe} and SP_{ZnS} + ZE LO_{ZnS}, as indicated in the figures. In addition to these optical phonons, disorder-induced acoustic phonons such as $2TA_{ZnSe}$ (transverse acoustic mode of ZnSe) and $2TA_{ZnS}$ (transverse acoustic mode of ZnS) are also observed. The strength of $2TA_{ZnS}$ phonon increases as the sulfur content increases. The strength of the $2TA_{ZnSe}$ phonon, however, appears to remain constant due to the increased scattering from the substrate at around 135 cm^{-1}. This occurs because of the decrease in thickness and absorption coefficient in the samples with larger fractions of sulfur.

The plot of intensity ratio of the two LO phonons $\left[\frac{I(LO_{ZnS})}{I(LO_{ZnSe})}\right]$ against the fraction of sulfur (x) is given in Fig. 10a. The plot shows that the relative strength of the zone centre phonons is dependent on the fraction of sulfur, as has been reported for other mixed crystals exhibiting two-mode behavior.[38] The intensity ratio $\left[\frac{I(LO_{ZnS})}{I(LO_{ZnSe})}\right]$ increases from 0.76 in $ZnS_{0.41}Se_{0.59}$ to 1.82 in $ZnS_{0.91}Se_{0.09}$. This corresponds to the increasing number of the Zn–S bond (decreasing number of the Zn–Se bond) in the mixed crystal as more anion sites in the crystal are occupied by S atoms.

Figure 10b shows the Raman shift of the first-order Raman modes plotted against the sulfur content (x). The TO_{ZnSe} and LO_{ZnSe} phonon mode frequencies, which are widely separated in the pure ZnSe sample, gets narrower with the increase in sulfur content. In the $ZnS_{0.91}Se_{0.09}$ sample, the TO_{ZnSe} and LO_{ZnSe} merge, resulting in a weak phonon at 221 cm^{-1}, which is the gap mode of Se in

the ZnS lattice as theoretically predicted.[14,16] In this sample, the small fraction of Se in the ZnS lattice vibrates at a frequency lower than the optical phonons of ZnS, thereby resulting in a phonon mode at the forbidden gap.

Our observation of asymmetric broadening in LO_{ZnS} phonon mode is a very interesting feature of ZnS_xSe_{1-x} ternary alloys, which, to our knowledge, has not previously been reported, though similar broadening in LO_{CdS} phonon modes has been reported in the Raman spectra of CdS_xSe_{1-x} thin films.[39,40] In nanocrystalline materials, the surface phonon modes could result in this asymmetric broadening, whereas in the case of thin films and single crystals of CdS_xSe_{1-x}, the contribution from zone edge LO phonon vibrations are believed to be responsible for the observed asymmetry.[39,40]

In our analysis of asymmetrically broadened LO_{ZnS}, we used the two-Lorentzian functions as proposed by both Pagliara et al.[39] and Ingale et al.[40] We observe that the frequency of additional Lorentzian peak shifts in the same manner as the zone
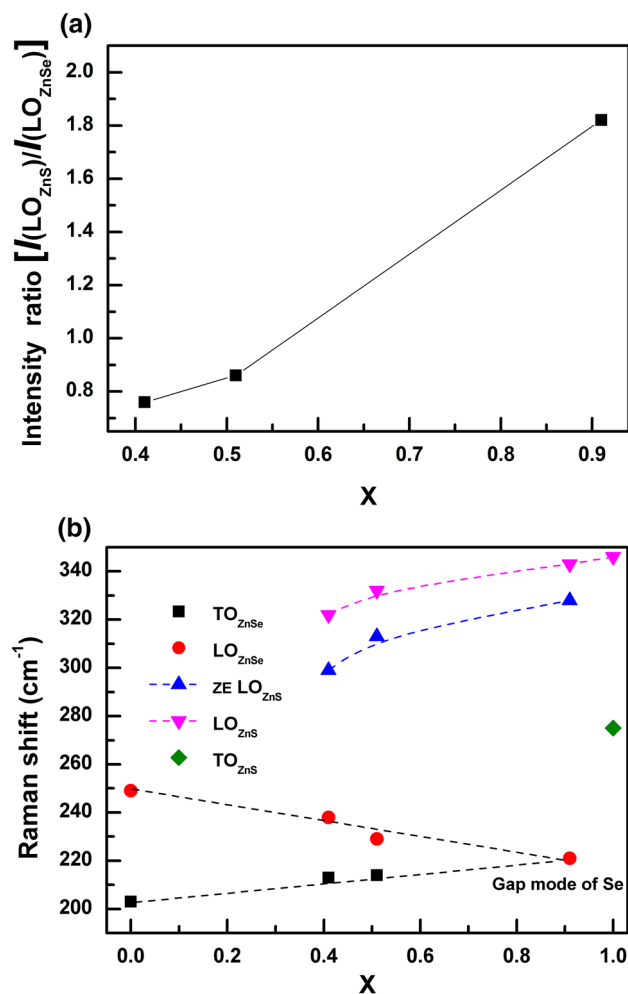

Fig. 10. (a) Plot of intensity ratio of the two LO phonons $\left[\frac{I(LO_{ZnS})}{I(LO_{ZnSe})}\right]$ versus fraction of sulfur (x), (b) plot of Raman shift versus fraction of sulfur (x).

centre phonon mode, as shown in Fig. 10b. For each of the ternary alloys, the Raman shift of the additional Lorentzian peak is about 20 cm^{-1} below the zone centre LO phonon mode and both increase with the sulfur atomic concentration. This additional Lorentzian peak is, thus, assigned to ZE LO$_{ZnS}$, and its origin can be understood from the dispersion curve of the binary compounds (ZnS and ZnSe).[41,42] In the dispersion curve of ZnS,[41] the LO$_{ZnS}$ and TO$_{ZnS}$ phonon modes are still widely separated at the zone boundaries forming distinct zone edge phonon vibrations, ZE LO$_{ZnS}$ and ZE TO$_{ZnS}$, respectively, at frequencies which are slightly different from the respective zone centre phonon modes. These phonon modes can become Raman-active once we have significant disorder. The ZE LO$_{ZnS}$ frequency being lower than the zone centre LO$_{ZnS}$ phonon for about 20 cm^{-1} [41] results in asymmetric broadening of LO$_{ZnS}$ on the lower wave number side as observed in our samples. However, in the dispersion curve of ZnSe,[42] the LO$_{ZnSe}$ phonon mode frequency falls down and merges with TO$_{ZnSe}$ phonon mode at the zone boundaries and results in a zone edge vibrational mode close to the zone centre TO$_{ZnSe}$ phonon mode, which cannot be distinguished. Thus, the zone edge phonon in ZnSe cannot be distinctly observed as in the case of ZE LO$_{ZnS}$ and, if it becomes Raman active, it would contribute to the TO$_{ZnSe}$.

The assigned Gaussian peaks in asymmetrically broadened binary compounds (ZnSe and ZnS) can also be explained from the above discussion. Since the asymmetric Gaussian peak in LO$_{ZnS}$ is very large, it could be due to the contributions from both ZE LO$_{ZnS}$ and the surface phonon (SP$_{ZnS}$) mode. However, since the zone edge contribution does not occur in ZnSe, a weak Gaussian peak as observed in the present case could be solely due to the surface phonon (SP$_{ZnSe}$) mode.

CONCLUSION

We have prepared ZnS$_x$Se$_{1-x}$ (x = 0, 0.41, 0.51, 0.91, 1) ternary alloy thin films with variable structural, optical and vibrational properties by employing a simple thermal evaporation route. The dependence of the lattice constant on the composition has a bowing parameter of 0.12 Å. Optical studies show the presence of SO splitting in the ZnS$_x$Se$_{1-x}$ ternary compounds having a significant contribution of Se, which has not been experimentally reported so far to the best of our knowledge. Even though the band structure of this ternary alloy has not been well understood, we are able to show that the relative fraction of anions in the alloy not only affects the bandgap but also determines the extent of SO splitting in the valence band. The vibrational properties of the ternary alloys exhibit two phonon mode behavior as predicted by a modified random element iso-displacement (MREI) model. The changes in Raman shift with the fraction of sulfur content follows the theoretically predicted pattern. The LO$_{ZnSe}$ and TO$_{ZnSe}$ phonon frequencies merge at 221 cm^{-1} in ZnS$_{0.91}$Se$_{0.09}$, forming the gap mode of Se in the ZnS lattice. To our knowledge, we are the first to experimentally report a Se gap mode in a ZnS$_x$Se$_{1-x}$ ternary system.

REFERENCES

1. P. Uusimaa, A. Salokatve, K. Rakennus, A. Rinta-Moykky, and M. Pessa, *Mater. Sci. Eng. B* 51, 18 (1998).
2. H.C. Lee, T. Abe, M. Watanabe, Z.M. Aung, M. Adachi, T. Shirai, H. Yamada, S. Kuroda, H. Kasada, and K. Ando, *J. Cryst. Growth* 214–215, 1096 (2000).
3. T.V. Shubina, S.V. Ivanov, A.A. Toropov, G.N. Aliev, M.G. Tkatchman, S.V. Sorokin, N.D. Il'inskaya, and P.S. Kopev, *J. Cryst. Growth* 184–185, 596 (1998).
4. K.S. Wong, T. Sun, B.K.K. Fung, I.K. Sou, and G.K.L. Wong, *J. Cryst. Growth* 227–228, 717 (2001).
5. Y.P. Venkatasubbaiah, P. Prathap, K.T. Ramakrishnareddy, R.W. Miles, and J. Yi, *Thin Solid Films* 516, 7060 (2008).
6. K.T. Ramakrishna Reddy, Y.V. Subbaiah, T.B.S. Reddy, D. Johnston, I. Forbes, and R.W. Miles, *Thin Solid Films* 431–432, 340 (2003).
7. S. Armstrong, P.K. Datta, and R.W. Miles, *Thin Solid Films* 403–404, 126 (2002).
8. Rong Rujkorakarn and Art J. Nelson, *J. Appl. Phys.* 87, 8557 (2000).
9. A.L. Gurskii, E.V. Lutsenko, G.P. Yablonskii, V.I. Kozlovsky, A.B. Krysa, J. Sollner, M. Sholl, H. Hamadeh, and M. Heuken, *J. Cryst. Growth* 159, 518 (1996).
10. C.T. Hsu, *Mater. Chem. Phys.* 58, 6 (1999).
11. J.R. Chelikowsky and M.L. Cohen, *Phys. Rev. B* 14, 556 (1976).
12. J.P. Walter, M.L. Cohen, Y. Petroff, and M. Balkanski, *Phys. Rev. B* 1, 2661 (1970).
13. Y.D. Kim, M.V. Klein, S.F. Ren, Y.C. Chang, H. Luo, N. Samarthi, and J.K. Furdyna, *Phys. Rev. B* 49, 7262 (1994).
14. I.F. Chang and S.S. Mitra, *Phys. Rev.* 172, 924 (1968).
15. S.N. Behera, P. Nayak, and Patnaik, *Pramana* 8, 255 (1977).
16. O. Brafman, I.F. Chang, G. Lengyel, and S.S. Mitra, *Phys. Rev. Lett.* 19, 1120 (1967).
17. G.S. Paul, P. Gogoi, P. Agarwal, and Gouri Sankar Paul, *J. Noncryst. Solids* 354, 2195 (2008).
18. G. Ramalingam, N. Melikechi, P. Dennis Christy, S. Selvakumar, and P. Sagayaraj, *J. Cryst. Growth* 311, 3138 (2009).
19. M. Ashraf, S.M.J. Akhtar, A.F. Khan, Z. Ali, and A. Qayyum, *J. Alloys Compd.* 509, 2414 (2011).
20. I. Langmuir, *Phys. Rev.* 2, 329–342 (1913).
21. A. Goswami, *Thin Film Fundamentals* (New Delhi: New Age International Limited, 1996), p. 17.
22. K.T. Jacob, Shubhra Raj, and L. Rannesh, *J. Mater. Res.* 98, 776 (2007).
23. B. Jobst, D. Hommel, U. Lunz, T. Gerhard, and G. Landwehr, *Appl. Phys. Lett.* 69, 97 (1996).
24. M. Ameri, D. Rached, M. Rabah, R. Khenata, N. Benkhettou, B. Bouhafs, and M. Maachou, *Mater. Sci. Semicond. Proc.* 10, 6 (2007).
25. G.K. Williamson and W.H. Hall, *Acta Metall.* 1, 22 (1953).
26. R. Swanepoel, *J. Phys. E* 16, 1214 (1983).
27. Y.P. Venkata Subbaiah, P. Prathap, M. Devika, and K.T. Ramakrishna Reddy, *Physica B* 365, 240 (2005).
28. A. Goudarzi, G.M. Aval, R. Sahraei, and H. Ahmadpoor, *Thin Solid Films* 516, 4953 (2008).

29. Biljana Pejova, *J. Solid State Chem.* 181, 1961 (2008).
30. T. Tsuchiya, S. Ozaki, S. Adachi, and J. Phys, *Condens. Matter* 15, 3717 (2003).
31. S. Velumani, X. Mathew, P.J. Sebastian, S.K. Narayandass, and D. Mangalaraj, *Sol. Energy Mater. Sol. Cells* 76, 347 (2003).
32. Y.-T. Nien, B. Zaman, J. Quyang, I.-G. Chen, C.-S. Hwang, and K. Yu, *Mater. Lett.* 62, 4522 (2008).
33. M. Cardona, *J. Phys.* 45, C8–29 (1984).
34. D. Huang, C. Jin, D. Wang, X. Liu, J. Wang, and X. Wang, *Appl. Phys. Lett.* 67, 3611 (1995).
35. M. Kozielski, M. Szybowicz, F. Rirszt, S. Legowski, H. Meczynska, J. Szatkowski, and W. Paszkowicz, *Cryst. Res. Technol.* 34, 699 (1999).
36. O. Madelung, M. Schulz, and H. Weiss, eds., Numerical Data and Functional Relationships in Science and Technology, Landolt-Bornstein, New Series, Group III, Vol. 17, Pt. b (Springer, Berlin, 1982).
37. A. Memon and D.B. Tanner, *Phys. Status Solidi B* 128, 49 (1985).
38. A. Tu and P.D. Persans, *Appl. Phys. Lett.* 58, 1506 (1991).
39. S. Pagliara, L. Sangaletti, L.E. Depero, V. Capozzi, and G. Perna, *Solid State Commun.* 116, 115 (2000).
40. A. Ingale and K.C. Rustagi, *Phys. Rev. B* 58, 7197 (1998).
41. B. Hennion, F. Moussa, G. Pepy, and K. Kunc, *Phys. Lett.* 36A, 376 (1971).
42. N. Vagelatos, D. Wehe, and J.S. King, *J. Chem. Phys.* 60, 3613 (1974).